Numerical modelling of ductile damage failure of butterfly specimen under combined shear and tension large deformations

B. ABBES[a], L. SIAD[b], S.C. GANGLOFF[b]

a. GRESPI, Université de Reims, UFR Sciences, Moulin de la Housse 51687 Reims.
boussad.abbes@univ-reims.fr
b. BIOS, Université de Reims, UFR Pharmacie, 1 rue du Maréchal Juin 51100 Reims.
larbi.siad@univ-reims.fr

Résumé :

Dans cette communication une extension du modèle élastoplastique avec écrouissage isotrope GTN (Gurson-Tvergaard-Needleman) est proposée. Le modèle de comportement proposé se différencie du modèle GTN par un potentiel plastique pré-existant qui a la particularité de dépendre explicitement du troisième invariant des contraintes. En outre, les constantes de Tvergaard varient avec la porosité du matériau considéré. Le modèle proposé est utilisé pour simuler numériquement le comportement à la rupture d'éprouvettes "butterfly" soumises à des chargements mixtes de cisaillement et de traction. Les résultats fournis par le modèle proposé et le modèle GTN sont très proches avant l'amorçage de la rupture en zone centrale de l'éprouvette. Cette observation est valable aussi bien pour les chargements à traction-dominante que pour les chargements à cisaillement dominant. Pour ces derniers, les résultats se distinguent dès le début de la rupture de l'éprouvette.

Abstract :

An extended version of the well-known GTN (Gurson-Tvergaard-Needleman) isotropic hardening model is proposed in this paper. The yield function of the proposed constitutive model possesses the distinctiveness to explicitly depend upon the third stress invariant. Besides, the Tvergaard parameters depend upon the void volume fraction. The proposed constitutive model is used to numerically analyze the failure behaviour of butterfly specimen. As long as softening initiation of specimen is not reached, the computational results highlight similarities and good agreement with those provided by the use of the GTN model. These observations hold for tension-dominated deformation and shear-dominated deformation as well. However, for the later loading, discrepancy shows up as soon as specimen failure starts.

Mots clefs : Ductile failure ; porous materials ; shear-dominated loading ; simulation.

1 Introduction

This investigation addresses the use of an extended version of the GTN isotropic hardening model (Gurson-Tvergaad-Needleman) to analyse the ductile failure behaviour of butterfly specimen subjected to combined shear and tension large deformations. The GTN model is the first micromechanical model introducing a strong coupling between deformation and damage [7, 5]. To put it in a nutshell, the material is assumed to be composed of a dense elastic-plastic matrix sprinkle with evenly distributed spherical microvoids. As regard failure behaviour, when the stress triaxiality (the ratio of the first to second stress invariants) is high enough, the voids remain near spherical and, as a matter of fact, the ductile fracture process is rather well described by the GTN model. On the other hand, if void nucleation is disregarded, this model cannot describe ductile damage evolution for shear-dominated loading. For such a loading for which stress triaxiality is low and even zero in case of pure shear, continued softening leading to ductile failure is known to occur [8, 4]. An extension of the GTN's plastic potential was proposed in [11] where the authors focused their study on the determination of yield surfaces for porous plastic materials using a huge number of finite element simulations. Rather the considered RVE was a cube containing a spherical void or parts of spherical voids. The obtained yield points was fitted by a new yield function which turned out to be similar to the Gurson one for porosity ranging between a very small value to the percolation threshold. This yield function was found to explicitly depend upon the third stress invariant.

In order to examine the effect of stress triaxiality and shear-dominated loading upon material failure, a constitutive GTN-like model based on the proposed plastic potential is numerically implemented in a finite element program. The presence of the third stress invariant in the yield function typically results in a high degree of non-linearity. The constitutive equations and the coalescence criterion based on the effective porosity are integrated using an algorithm based on the return mapping method. The proposed model is then used to analyze the behavior of a three-dimensional optimized butterfly specimen [10] subjected to shear-dominated and tension-dominated deformation, resulting in low and high stress triaxialities in the middle section of the specimen, respectively. The calculations have been carried out in Abaqus/Explicit and similar values for the damage parameters have been used for both the proposed model and the GTN one in order to compare their ability to predict void growth to coalescence and the corresponding failure mechanism. The problem formulation and numerical method follow that in [14] where further details and additional references are given. Cartesian tensor notation is used and the origin of the coordinate system is taken to be at the center of the specimen.

2 Problem formulation

2.1 Constitutive relations

An extension of the GTN's plastic potential with no extra parameters which fits the numerical data well and is valid for all void volume fractions and triaxial stress states has been proposed in [11]. The porous ductile materials contain spherical empty voids arranged in

cubic arrays, *namely*, simple cubic (SC), Body-Centred Cubic (BCC) and Face-Centred Cubic (FCC) arrays. FEA was used to simulate unit cells and the macroscopic yield surfaces of the porous materials were obtained using the probing technique which goal is to obtain a yield function in an analytical expression that can be used in continuum studies. The matrix material is almost rigid, perfectly plastic and unit cells were meshed with cubes. Depending on the unit cell at hand, the void volume fractions f considered range from 0.02 to around 0.90 (percolation threshold of the matrix material). For more detailed explanations of the subject, the reader are referred to the paper [11].

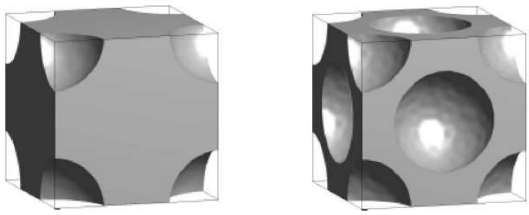

(a) BCC microstructure (b) FCC microstructure

FIGURE 1 – Two cubic unit cells, (Courtesy of A.P. Roberts [11]).

Let I_3 and J_3 be the determinant of the stress tensor $\boldsymbol{\sigma}$ and the third stress invariant of the deviatoric stress tensor $\boldsymbol{\sigma}'$, respectively : $\mathrm{I}_3 := \det(\boldsymbol{\sigma})$, $J_3 := \frac{1}{3}\,\mathrm{tr}\,\boldsymbol{\sigma}'^3$. I_3 and J_3 are related by $I_3 = J_3 + \frac{1}{3}\,p\,q^2 - p^3$. The approximate Gurson-Tvergaard-like condition proposed in [11] reads

$$\begin{aligned}\Phi(\boldsymbol{\sigma};\mathbf{H};s) = \; & \left(\frac{q}{\bar{\sigma}}\right)^2 + 2\,a_1(f)\,\cosh\left(-\frac{3\,a_2(f)\,p}{2\,\bar{\sigma}}\right) - 1 - a_1(f)^2 \\ & + s(f)\,\frac{p}{\bar{\sigma}}\left(\frac{\mathrm{I}_3}{\bar{\sigma}^3} + \frac{p^3}{\bar{\sigma}^3} + \frac{1}{3}\,\frac{p}{\bar{\sigma}}\left[2\,a_1(f)\cosh\left(-\frac{3\,a_2(f)\,p}{2\bar{\sigma}}\right) - 1 - a_1(f)^2\right]\right) = 0\end{aligned} \tag{1}$$

where the macroscopic Cauchy stress tensor $\boldsymbol{\sigma}$ is resolved as $\boldsymbol{\sigma} = -p\mathbb{1} + \frac{2}{3}\,q\,\mathbf{n}$ with $\mathbf{n} = \frac{3}{2}\frac{\boldsymbol{\sigma}'}{q}$ where $p = -\frac{1}{3}\,\mathrm{tr}\,\boldsymbol{\sigma}$ represents the hydrostatic pressure, $\mathbb{1}$ is the second order identity tensor, $\boldsymbol{\sigma}'$ is the deviatoric stress tensor, and $q = \left(\frac{3}{2}\,\boldsymbol{\sigma}' : \boldsymbol{\sigma}'\right)^{1/2}$ is the von Mises stress. In (1) f is the volume fraction of voids, $\bar{\sigma}$ is the effective flow stress of the damage-free matrix material which is a function of the effective plastic strain $\bar{\epsilon}^p$, (q_1, q_2) are the Tvergaard parameters, and $\mathbf{H} = (H_1, H_2)$ is a vector comprising the scalar state variables $H_1 = \bar{\epsilon}^p$ and $H_2 = f$.

In stress space (p, q, I_3), yield points were found by monotonically increasing macroscopic strain with fixed ratios until the macroscopic equivalent stress reaches a maximum. For each of the three cubic unit cells, a least-squares fit with an extension of the GTN's yield function was found only approximately with deviations becoming more pronounced as pressure p or void volume fraction f were increased. Note that for the extended yield function Φ given by (1), the Tvergaard q-like parameters a_1 and a_2 depend on f, that is $a_1 = a_1(f)$, $a_2 = a_2(f)$. It linearly depends upon the third stress invariant I_3 with coefficient proportional to the hydrostatic pressure p. The parameter s, also depending on f, determines the influence of the new term in the yield condition (1) which reduces to that of the classical GTN model for $s = 0$, $a_1 = q_1\,f$ and $a_2 = q_2$. Whenever the constant s is non-zero, there is an effect of I_3 on the plastic flow. Clearly the yield function Φ contains three functions of void-volume fraction f, *namely* a_1, a_2 and s which are slightly different for each of the three cubic microstructures considered in [11].

The constitutive equations can be written in a rate format as

$$\dot{\boldsymbol{\epsilon}} = \dot{\boldsymbol{\epsilon}}^e + \dot{\boldsymbol{\epsilon}}^p\;,\; \dot{\boldsymbol{\sigma}} = \mathbf{C}^e : (\dot{\boldsymbol{\epsilon}} - \dot{\boldsymbol{\epsilon}}^p)\;,\; \dot{\boldsymbol{\epsilon}}^p = \dot{\lambda}\,\mathbf{r}(\boldsymbol{\sigma};\mathbf{H})\;,\; \dot{\mathbf{H}} = \dot{\lambda}\,\mathbf{h}(\boldsymbol{\sigma};\mathbf{H}) \tag{2}$$

where $\mathbf{C}^e$ is the elastic moduli tensor, $\mathbf{r}$ is the direction of the plastic flow which depends on the current stress and on a finite set of plastic internal variables $\mathbf{H}$ accounting for history effects and $\mathbf{h}$ is the direction of the rate of these plastic internal variables. In associated plasticity, $\mathbf{r}$ is the gradient of the yield function Φ :

$$r_{ij}\left(\sigma;\mathbf{H}\right)=\frac{\partial\Phi}{\partial\,\sigma_{ij}}(p,q,J_3;\mathbf{H})=-\frac{1}{3}\,\frac{\partial\Phi}{\partial p}\,\delta_{ij}+\frac{3}{2\,q}\,\frac{\partial\Phi}{\partial q}\,\sigma'_{ij}+\frac{\partial\Phi}{\partial J_3}\,\sigma'_{ik}\,\sigma'_{kj}-\frac{2}{9}\,\frac{\partial\Phi}{\partial J_3}\,q^2\,\delta_{ij} \tag{3}$$

The plastic strain rate, Eq. $(2)_3$, is trivially decomposed into volumetric and deviatoric parts, $\dot{\boldsymbol{\epsilon}}^p=\dfrac{1}{3}\,\dot{\epsilon}^p_v\,\mathbb{1}+\dot{\boldsymbol{\epsilon}}^p_q$, which facilitates development of the integration algorithm :

$$\dot{\epsilon}^p_v=-\dot{\lambda}\,\frac{\partial\Phi}{\partial p}\ \text{and}\ \ \dot{\boldsymbol{\epsilon}}^p_q=\dot{\lambda}\left(\frac{\partial\Phi}{\partial\boldsymbol{\sigma}'}-\frac{2}{9}\,\frac{\partial\Phi}{\partial J_3}\,q^2\,\mathbb{1}\right) \tag{4}$$

It should be noted at this stage of calculation that, due to the presence of the third stress invariant J_3 in the expression of the yield function Φ, and in view of expression $(3)_2$, the deviatoric component $\dot{\boldsymbol{\epsilon}}^p_q$ cannot be put in the form $\dot{\boldsymbol{\epsilon}}^p_q=\dot{\epsilon}^p_q\,\mathbf{n}$, where $\mathbf{n}$ is the deviatoric strain rate tensor normal to the yield surface $\Phi=0$ and which norm is unity. This form has turned out to be very successful for applying the implicit integration scheme based on the Aravas's method [2].

The current effective stress governing flow of the damage-free matrix material $\bar{\sigma}$ which is a function of the von Mises accumulated plastic strain $\bar{\epsilon}^p$, through the hardening law $\bar{\sigma}=\bar{\sigma}(\bar{\epsilon}^p)$. The *effective* void volume fraction $f^\star$ was intended to simulate the rapid loss of strength accompanying void coalescence. To determine the plastic multiplier, the loading unloading conditions should be imposed in a Kuhn-Tucker form as

$$\dot{\lambda}\geq 0,\quad \Phi(p,q,J_3;\mathbf{H})\leq 0,\quad \dot{\lambda}\,\Phi(p,q,J_3;\mathbf{H})=0 \tag{5}$$

implying that during plastic loading, $\Phi=0$, $\dot{\lambda}\geq 0$ and $\dot{\Phi}=0$. This condition (consistency condition) allows the determination of the plastic multiplier which specifies the magnitude of the plastic strain rate [6, 1, 15].

2.2 Stress integration algorithm

The computed porous plastic material response is strongly dependent on the computational procedure for stress calculation, usually called the stress integration. The presence of the third stress invariant J_3 in the yield condition (1) typically results in a high degree of non-linearity and thereby an adapted numerical algorithms. Implicit solution strategies for

models depending on the third stress invariant have been developed, in particular, for models of general isotropic elasto-plastic geomaterials [6]. Generally speaking, regarding elasto-plastic material, the incremental-iterative analysis consists in dividing up the applied load into a number of small increments, and within each increment, iterations are performed. The final stress and hardening parameters are determined solving the non-linear equations iteratively so that the stress increment fulfills the consistency condition. Herein, a stress integration algorithm based on the general backward-Euler return algorithm [6, 1, 15] has been developed and implemented into Abaqus/Explicit [14]. Box right summarizes the main steps of the algorithm. The programmed user subroutine Vumat is then called by the FE code at each element integration point, for each increment, and during each load step.

❶ Initialization
  (a) Establish $\Delta\boldsymbol{\epsilon}, \mathbf{H}_t, \boldsymbol{\sigma}_t, \text{Stol}, \text{Stol}_v, \text{Stol}_H, \text{Stol}_\Phi$, and $\text{N}_\text{L}^{\max}$;
  (b) Establish the constitutive model parameters;
  (c) Set $\text{N}_\text{L} = 0$ and $\mathbf{H}_{t+\Delta t} = \mathbf{H}_t$
❷ Compute elastic predictor $\boldsymbol{\sigma}^T_{t+\Delta t}$, and $\Phi^T := \Phi(\boldsymbol{\sigma}^T_{t+\Delta t}; \mathbf{H}_{t+\Delta t})$.
  (a) Perform loading/unloading check.
  (b) If $(\Phi < \text{Stol})$, set $\boldsymbol{\sigma}_{t+\Delta t} = \boldsymbol{\sigma}^T_{t+\Delta t}$ and go to step ❾
❸ Set $\boldsymbol{\sigma}_{t+\Delta t} = \boldsymbol{\sigma}^T_{t+\Delta t}$ and calculate $\mathbf{r}_{t+\Delta t}$ and $\left(\frac{\partial \Phi}{\partial \mathbf{H}_{t+\Delta t}}\right).\mathbf{h}$.
❹ Set $R^{(1)}_\Phi = \Phi^T$
  (a) Compute initial value for $\Delta\lambda$;
  (b) Compute $\boldsymbol{\sigma}_{t+\Delta t}$ and $\mathbf{H}_{t+\Delta t}$;
  (c) Set $\boldsymbol{\sigma}_{t+\Delta t} = \boldsymbol{\sigma}^{(1)}_{t+\Delta t}$ and $\mathbf{H}_{t+\Delta t} = \mathbf{H}^{(1)}_{t+\Delta t}$.
❺ Begin iterations
  (a) Compute $R^{(1)}_\Phi = \Phi(\boldsymbol{\sigma}_{t+\Delta t}, \mathbf{H}_{t+\Delta t})$ and $\mathbf{r}_{t+\Delta t}$;
  (b) Compute $\boldsymbol{\sigma}^{(2)}_{t+\Delta t}$ and $\mathbf{H}^{(2)}_{t+\Delta t}$;
  (c) Compute $\mathbf{R}^{(1)}_v := \boldsymbol{\sigma}^{(2)}_{t+\Delta t} - \boldsymbol{\sigma}^{(1)}_{t+\Delta t}$ and $\mathbf{R}^{(1)}_H := \boldsymbol{\sigma}^{(1)}_{t+\Delta t} - \boldsymbol{\sigma}^{(2)}_{t+\Delta t}$.
❻ Find errors $\text{e}_\infty, \text{e}_\text{H}$ and e_Φ.
  (a) Perform convergence check;
  (b) If converged go to step ❾.
❼ Set $\text{N}_\text{L} \leftarrow \text{N}_\text{L} + 1$
  • If $\text{N}_\text{L} > \text{N}_\text{L}^{\max}$, STOP.
  • If converged go to step ❾.
❽ Compute $\delta\lambda, \delta\boldsymbol{\sigma}$ and $\delta\mathbf{H}$.
  (a) Update $\boldsymbol{\sigma}^{(1)}_{t+\Delta t} \leftarrow \boldsymbol{\sigma}^{(1)}_{t+\Delta t} + \delta\boldsymbol{\sigma}$, $\mathbf{H}^{(2)}_{t+\Delta t} \leftarrow \mathbf{H}^{(1)}_{t+\Delta t} + \delta\mathbf{H}$ and $\Delta\lambda^{(1)}_{t+\Delta t} \leftarrow \Delta\lambda^{(1)}_{t+\Delta t}$;
  (b) Set $\boldsymbol{\sigma}_{t+\Delta t} = \boldsymbol{\sigma}^1_{t+\Delta t}$ and $\mathbf{H}_{t+\Delta t} = \mathbf{H}^1_{t+\Delta t}$;
  (c) Go to step ❺.
❾ Return to the main program

3 Butterfly specimen under shear and tensile loading

The geometry of the butterfly specimen, proposed and designed by Bai and Wierzbicki [3] and Mohr and Henn [12], is such that fracture triggers within the flat large central area of the gage section. Consequently, the start failure zone is then remote from the lateral free edges. This geometry exhibits an abrupt change in thickness between the gage section and the specimen shoulders. The distinctive features of the optimized geometry obtained by Dunand and Mohr [10] is a gage section of reduced thickness bounded by shoulders of clothoid shape. As a result, wide range of stress and strain states within the middle gage section can be displayed by simultaneously loading the top and bottom of the specimen boundaries, horizontally and/or vertically. Fig. 2 shows a schematic representation of the geometry of the specimen under consideration. Hereafter, calculations are performed on steel alloys in order to determine the stress and strain fields within the specimen gage section. Numerous and various loading conditions, ranging from pure shear to transverse plane strain tension, are considered.

• **Loading conditions** : the bottom face of the specimen $x = -H_o/2$ is maintained fixed, whereas the top face $x = H_o/2$ is subject to a controlled displacement. If the specimen is horizontally loaded, a pure shear stress state is obtained, while an approximate plane strain tension or compression, depending on the load direction, is obtained by loading the specimen vertically. The controlled displacement is expressed as $\mathbf{u} = u_x\mathbf{e}_x + u_y\mathbf{e}_y$ with $u_x = \alpha\, u_y$,

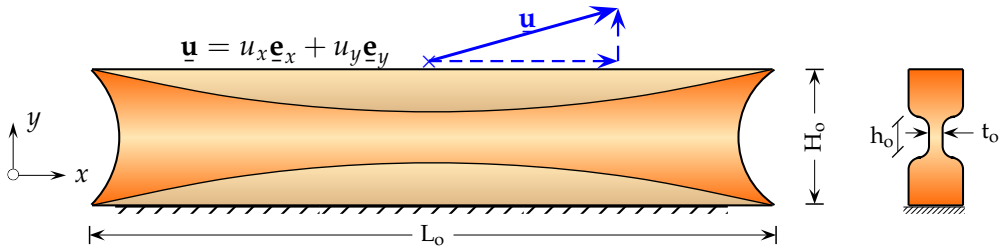

FIGURE 2 – Schematic representation of the geometry and loading of a butterfly specimen, (adapted from Refs. [10, 9])

$(0 < \alpha < 1)$ for shear-dominated deformation loading, and $u_y = \beta u_x$, $((0 < \beta < 1)$ for tension-dominated deformation loading. The biaxial loading parameters α and β are kept constant along the whole process of deformation. In short, the boundary conditions can be expressed as follows :

$$\mathbf{u}(x, H_o/2, t) = u_x \mathbf{e}_x + u_y \mathbf{e}_y \,, \quad \mathbf{u}(x, -H_o/2, t) = \mathbf{0} \,, \quad 0 \leq t < T. \tag{6}$$

where the components u_x and u_y are proportional and T is the time period of the analysis. In this communication, the addressed loading conditions of the butterfly specimen are as follows : (i) we start with a pure shear loading with a controlled displacement given then by $\mathbf{u}(x, H_o/2, t) = u_x^f \mathbf{e}_x$ with $u_x^f > 0$; In this circumstance, stress triaxialities in the vicinity of the middle section of the specimen are expected to be very close to zero (at least before localization occurs) ; (ii) afterwards, a uniaxial tension loading is considered. The corresponding smoothly controlled displacement is given by $\mathbf{u}(x, H_o/2, t) = u_y^m \mathbf{e}_y$ where $u_y^m > 0$. On the contrary of the previous loading condition, uniaxial tension load results in higher stress triaxialities in the vicinity of the middle section of the specimen. The magnitude of u_x^m (shear loading) and u_y^m (tension loading) are determined by trial and error ; (iii) the specimen is also subject to a set of six loading paths starting with a shear-dominated deformation loading ($\alpha = 0.10$) and for which $\alpha = 0.10, 0.20, 0.30, 0.60, 0.80$ and 0.90. As a matter of fact, according to Danas and Aravas [9], a shear-dominated deformation loading is attained through the choice of $\alpha = 0.10$; (iv) the final considered loadings consist in a set of six loading paths starting with a tension-dominated deformation loading ($\beta = 0.10$) and for which $\beta = 0.10, 0.20, 0.30, 0.60, 0.80$ and 0.90.

• **Materials** : the sound matrix of the porous material at hand is assumed to exhibit isotropic work-hardening characteristics following the power law $\bar{\sigma}/\sigma_o(\bar{\epsilon}^p) = \left(1 + E\,\bar{\epsilon}^p/\sigma_o\right)^N$, where σ_o denotes the initial yield stress, E is the Young's modulus, and N is the strain hardening exponent. The used values for these parameters are $E/\sigma_o = 300$, and $N = 0.1$; as for the Poisson's ratio, it is taken to be $\nu = 0.3$ [9]. The matrix phase is considered to be initially unloaded with zero accumulated plastic strain $\bar{\epsilon}^p = 0$. The material properties including the stress-strain curve and the damage parameters employed for the description of the porous material are conveniently listed in Table 1 : the initial porosity is taken to be $f_o = 0.01$; the Tvergaard parameters q_1 and q_2 have been fixed to typical values suggested in literature ; f_c and f_f are the coalescence parameters accounting for rapid decrease in strength as neighbouring voids coalesce at failure.

• **Simulation** : the finite strain setting of Abaqus/Explicit platform is used to calculate the

TABLE 1 – Material parameters and geometrical constants of the butterfly specimen [9]

Material parameters :	$\bar{\sigma}/\sigma_o(\bar{\epsilon}^p) = \left(1 + E\,\bar{\epsilon}^p/\sigma_o\right)^N$
	$E/\sigma_o = 300.0, \quad \nu = 0.3, \quad \mathrm{N} = 0.10, \quad \rho = 7830\,\mathrm{kg/m^3}$
	$f_o = 0.01, \quad q_1 = 1.5, \quad q_2 = 1.0, \quad q_3 = 2.25, \quad f_c = 0.067, \quad f_f = 0.20$
Simulation constants :	$\mathrm{H_o} = 12.6\,\mathrm{mm}, \quad \mathrm{L_o} = 62.1\,\mathrm{mm}, \quad \mathrm{h_o} = 2.0\,\mathrm{mm}, \quad \mathrm{t_o} = 0.4\,\mathrm{mm}$
	$5 \times 10^{-3}s \leq$ Time period $\leq 6 \times 10^{-3}s$

stress and strain fields within the butterfly specimen and also to trace their histories in the vicinity of failure initiation. All calculations are performed under quasi-static conditions with a time period band of 5×10^{-3} to $6 \times 10^{-3}s$, depending on the situation under consideration (present constitutive model, GTN model, as well as loading conditions). Exploiting the symmetry of the butterfly specimen geometries, only half of its thickness is discretized. Reduced integration 3D hybrid (*i.e.*, with constant pressure) solid element C3D6R (8-noded cubic linear element) has been choosen to mesh the 3D geometry of the specimen. Preliminary calculations have showed that very fine mesh is needed to provide an accurate estimation of stress and strain fields. An assessment of the effect of the mesh refinement, regarding convergence and simulation time, has resulted in about 446300 elements for a typical mesh. This is indeed a highly refined mesh.

4 Numerical results and discussion

Hereafter, results based on the present constitutive model and the GTN one are compared, for the above stated loading conditions, in order to evaluate the predictive capabilities of the former. The loading paths to fracture of specimens are determined in terms of displacements. For each calculation, (i) tangential force RF_x versus horizontal displacement u_x curves, and (ii) axial force RF_y versus vertical displacement u_y curves. are recorded. Figure 3(a) depicts

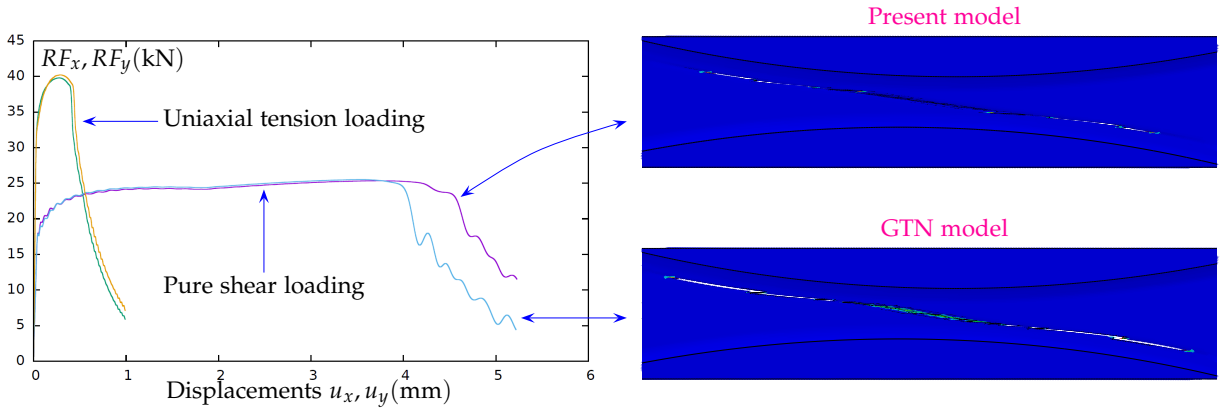

FIGURE 3 – (a) Force-displacement curves obtained for both present and GTN constitutive models when the butterfly specimen is subject to uniaxial tension and pure shear loadings. (b) Failure modes under pure shear loading.

the force-displacement curves predicted by both models for pure shear (right curves) and uniaxial tension (left curves) loadings. For the sake of space, Fig. 3(b) only shows the void volume fraction contour corresponding to the almost total failure of the butterfly specimen under pure shear deformation ($\alpha = 0$). It should be noted that in all performed calculations, plastic deformation localizes within the gage section prior to fracture. It can be seen from

Fig. 3(a) that for high stress triaxiality (tension deformation), the present constitutive model gives quite similar predictions as the GTN model. The $F_y - u_y$ curves exhibit a peak preceding a fast drop of the force, which could occur simultaneously with the onset of localized deformation. For very low stress triaxiality (shear deformation) the behaviour is qualitatively the same ; indeed, up to the failure initiation of the specimen, the predictions incorporating the present model are also in a close agreement with those provided by the GTN model. Theses results could confirm the potential of the former model to fulfill to the requirement of transferability between different loading conditions. However, there is a significant difference at and beyond failure points of specimen.

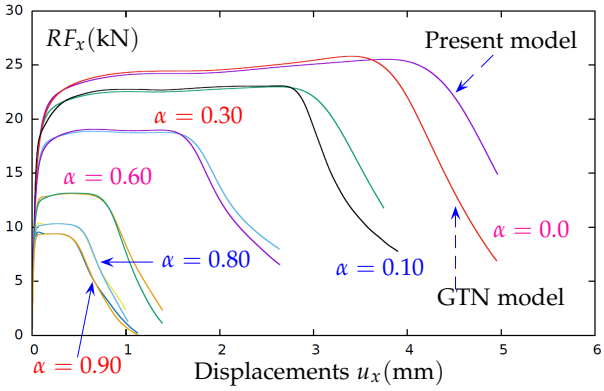

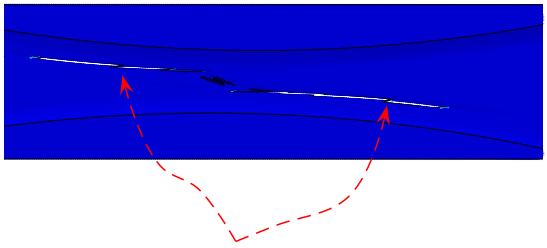

Failed shear bands developed within the central area of the gage section. The shear-dominated loading corresponds to $\alpha = 0.10$.

FIGURE 4 – (a) Comparison of force-displacement curves obtained for both present and GTN constitutive models : the butterfly specimen is subject to various loadings for which the load parameter α ranges from 0.1 (shear-dominated deformation) to 0.9 (tension-dominated deformation). (b) Failure modes under shear-dominated deformation with $\alpha = 0.1$.

Similar results are presented in Fig. 4(a) for six loadings ranging from shear-dominated deformation ($\alpha = 0.1$) to tension-dominated deformation ($\alpha = 0.9$), including the aforementioned loadings. For shear-dominated deformation, namely $0 \leq \alpha \leq 0.3$, the obtained force-displacement curves display a "plateau" which extent depends on the loading parameter α. Higher the value of this parameter, wider the extent of the "plateau". By way of illustration, Fig. 4(b) shows the void volume fraction contour corresponding to the almost total failure of the butterfly specimen under shear-dominated deformation with $\alpha = 0.1$.

5 Conclusion

The main objective of this communication has been to address an extended version of the GTN model based on a pre-existing yield function for porous plastic materials proposed in [11] and its implementation within a finite element code. To this end, a fully implicit stress integration scheme has been chosen. Similar values for the material parameters (elasticity, hardening, Tvergaard parameters, and coalescence parameters) have been used for both the present model and the GTN model in order to compare their ability to predict fracture of an optimized butterfly specimen [9, 10]. The obtained computational results may be briefly summarized as follows :

- For all performed calculations, using the proposed constitutive model and the GTN model for comparison purpose, plastic deformation localizes within the gage section prior to initiation of fracture faithfully in his zone.

- At high stress triaxialities (tension-dominated deformation), the proposed constitutive model gives similar predictions as the GTN model. Indeed, up to the failure initiation of the specimen, the predictions incorporating the present model are in a close agreement with those provided by the GTN model. This observation insists the potential of the former constitutive model to fulfill to the requirement of transferability between different loading conditions.
- For shear-dominated loading, at and beyond failure points of specimen, noticeable disagreement has been observed between predictions of both models.

Références

[1] A. Anandarajah, Computational Methods in Elasticity and Plasticity. Solids and Porous Media, Springer-Verlag, New York, 2010.

[2] N. Aravas, On the numerical integration of a class of pressure-dependent plasticity models. Int. J. Numer. Meth. Engng., 24 (1987), 1395–1416.

[3] Y. Bai, T. Wierzbicki, Application of extended Mohr-Coulomb criterion to ductile fracture, International Journal of Fracture, 161 (2010), 1–20.

[4] I. Barsoum, J. Faleskog, Rupture in combined tension and shear : Experiments, International Journal of Solids and Structures, 44 (2007), 1768-1786.

[5] A.A. Benzerga, J.-B. Leblond, Ductile Fracture by Void Growth to Coalescence, Advances in Applied Mechanics, 44 (2010), 169-305.

[6] R. Borja Plasticity. Modeling and computations Springer Dordrecht, 2013.

[7] L. Chen, C. Butcher Micromechanics modelling of ductile fracture, Springer Dord., 2013.

[8] J.G. Cowie, M. Azrin, G.B. Olson, Microvoid formation during shear deformation of ultrahigh strength steels, Metallurgical Transaction A, 20A (1989), 143–153.

[9] K. Danas, N. Aravas, Numerical modeling of elasto-plastic porous materials with void shape effects at finite deformations, Composites-Part B, 43 (2012) 2544-2559.

[10] M. Dunand, D. Mohr, Optimized butterfly specimen for the fracture testing of sheet materials under combined normal and shear loading, Engineering Fracture Mechanics, 78 (2011), 2919–2934.

[11] D.L. Sean McElwain, A.P. Roberts, A.H. Wilkins, Yield criterion for porous materials sujected to complex stress states, Acta materialia, 54 (2006).

[12] D. Mohr, S. Henn, Calibration of stress-triaxiality dependent crack formation criteria : a new hybrid experimental-numerical method, Exp. Mechanics, 47 (2007), 805–820.

[13] K. Nahshon, J. Hutchinson, Modification of the Gurson model for shear failure, European Journal of Mechanics A/Solids, 27 (2008), 1–17, 2008.

[14] L. Siad, Ductile damage analysis based on a J_3-GTN-like model, Journal of Multiscale Modelling, 3 (2011), 1–27.

[15] J. Simo, T.J.R., Hughes, Computational inelasticity, Springer-Verlag, New York, 1998.